NANO · MICRO small

www.small-journal.com

Tubular 3D Resistive Random Access Memory Based on Rolled-Up *h*-BN Tube

Xiang Hou, Ruobing Pan, Qiang Yu, Kai Zhang, Gaoshan Huang, Yongfeng Mei, David Wei Zhang, and Peng Zhou**

Due to their advantages compared with planar structures, rolled-up tubes have been applied in many fields, such as field-effect transistors, compact capacitors, inductors, and integrative sensors. On the other hand, because of its perfect insulating nature, ultrahigh mechanical strength and atomic thickness property, 2D hexagonal boron nitride (*h*-BN) is a very suitable material for rolled-up memory applications. In this work, a tubular 3D resistive random access memory (RRAM) device based on rolled-up *h*-BN tube is realized, which is achieved by self-rolled-up technology. The tubular RRAM device exhibits bipolar resistive switching behavior, nonvolatile data storage ability, and satisfactorily low programming current compared with other 2D material-based RRAM devices. Moreover, by releasing from the substrate, the footprint area of the tubular device is reduced by six times. This tubular RRAM device has great potential for increasing the data storage density, lowering the power consumption, and may be applied in the fields of rolled-up systems and sensing-storage integration.

In recent years, self-rolled-up 3D compact structures have inspired many studies.[1–5] As a typical representative structure, rolled-up tubes have been constructed and applied in many fields, such as compact capacitors,[1,6] field-effect transistors,[7] lithium ion batteries,[8,9] 3D inductors,[10] and integrative sensors.[5,11] Different from flexible devices, rolled-up tubes exhibit greater deformation (complete tubular structure with more than one winding) and have no requirement for flexibility of the substrate. These rolled-up devices have various advantages (such as smaller footprint area,[1,6] higher energy density, versatility,[7] etc.) compared with normal planar devices, and the devices have great potential to be integrated into circuits for further electrical processing and demonstrations. However, no rolled-up memory device has been demonstrated yet, which is indispensable for information storage in a rolled-up system and has great potential for sensing-storage integration in More-than-Moore applications. Thus, tubular rolled-up nonvolatile memory device is urgently demanded for device integration and system optimization for practical applications.

With the shrinking of semiconductor technology nodes, metal-oxide-semiconductor filed-effect transistors based flash memory cells are approaching their physical limits, such as the exponentially increased leakage current and weak charges storage capability.[12] On the contrary, resistive random access memory (RRAM) due to the reducible metal-insulator-metal (MIM) structure is considered as one of the most promising candidates for the next-generation nonvolatile memory application with desirable scalability.[13–16] Therefore, an RRAM device is the better choice for rolled-up application. At present, many transition metal oxides (TMOs), such as Al_2O_3,[17,18] HfO_2,[19,20] etc., have been found to have stable nonvolatile resistive switching ability in the planar MIM structure. However, probably because the mechanical strength of TMOs is not strong enough, resistive switching behavior is difficult to realize in rolled-up TMO tubes, which is verified by our experiments (see more details in Section S1 in the Supporting Information).

Fortunately, due to their ultrahigh mechanical strength[21,22] and atomic thickness property,[23] 2D materials are suitable for rolled-up applications. As an ideal 2D insulator,[24] hexagonal boron nitride (*h*-BN) has a large bandgap of ≈5.5 eV[25,26] and the dielectric constant is about 3.[27] Moreover, the desirable resistive switching ability of *h*-BN has been proved with an ideal current ON/OFF ratio,[28,29] because of the perfect insulating nature, dangling bonds-free surface, and excellent chemical stability.[30,31]

In this work, nonvolatile RRAM device based on rolled-up *h*-BN tube was demonstrated via self-rolled-up technology. Titanium (Ti) and chromium (Cr) were employed as the metal

Dr. X. Hou, Prof. D. W. Zhang, Prof. P. Zhou
State Key Laboratory of ASIC and System
School of Microelectronics
Fudan University
Shanghai 200433, China
E-mail: pengzhou@fudan.edu.cn

Dr. R. Pan, Prof. G. Huang, Prof. Y. Mei
Department of Materials
Fudan University
Shanghai 200433, China
E-mail: yfm@fudan.edu.cn

Dr. Q. Yu, Prof. K. Zhang
Suzhou Institute of Nano-Tech and Nano Bionics
CAS
Jiangsu 215123, China

The ORCID identification number(s) for the author(s) of this article can be found under https://doi.org/10.1002/smll.201803876.

DOI: 10.1002/smll.201803876

electrode and the strained layers in the rolling-up process, and chemical vapor deposition (CVD)-grown *h*-BN acted as the resistive switching layer. The rolled-up 3D tubular structure resulted in a footprint area reduction of ≈6 times by releasing from the substrate. Meaningfully, the tubular memory device exhibited forming-free bipolar resistive switching behavior with a nonvolatile memory performance. The ON/OFF ratio of the memory device could reach up to 10^3 with a stable retention property, and the programing current was satisfactorily low compared with other 2D material-based RRAM devices. The rolled-up tubular RRAM has the potential for increasing the data storage density, lowering the power consumption, and may be applied in the fields of rolled-up system and sensing-storage integration.

The self-rolled-up technology is responsible for the decrease in the device's footprint area and has the potential for increasing data storage density per footprint area. In this work, we have successfully introduced the self-rolled-up technology into the RRAM device based on 2D *h*-BN. The fabrication steps of the rolled-up tubes are illustrated in Figure S2a in the Supporting Information. First, a 15 nm thick Ge sacrificial layer was deposited on the top of the Si/SiO_2 substrate, which can be selectively removed by H_2O_2.[32,33] The gold can reduce the adhesion between the stacked layers and Ge sacrificial layer.[1] On the other hand, the strained Ti deposited by e-beam evaporation can provide stable stress in the rolling-up process.[6] Thus, the Au/Ti stack was employed as the first strained layer on the Ge sacrificial layer with thickness of 2 and 15 nm, respectively. Then, the multilayer *h*-BN film was transferred onto the sample via wet-transfer process, the details are illustrated in Figure S3 in the Supporting Information and the Experimental Section. After the *h*-BN transfer, the second strained Cr metal plate was deposited. The next fabrication step was the transfer of the second layer *h*-BN onto the Cr plate, which is necessary to prevent the short circuit between the Ti electrode and the Cr electrode after the rolling-up process. In order to ensure that the H_2O_2 can come into contact with the Ge sacrificial layer in the rolling-up process, a trench is necessary. To form the trench, the *h*-BN was selectively removed by reactive ion etching (RIE) in a CF_4/Ar atmosphere. Finally, the planar structural device was immersed in H_2O_2 solution (H_2O_2:H_2O = 1:50) at room temperature to remove the Ge sacrificial layer and release from the substrate.

The tubular structure of the rolled-up device is shown in **Figure 1**a, two contact pads were bonded on the substrate for the electrical measurement after device fabrication. The illustration on the right of Figure 1a is the partial enlargement 3D schematic view of the rolled-up *h*-BN tube, multilayer *h*-BN is caught between the Ti and Cr electrodes. To briefly describe the rolling-up process, the transformation of the device in the H_2O_2 solution is shown in Figure 1b. When the Ge sacrificial layer is slowly etched away, the strained Ti and Cr layer force the planar device to release from the substrate. Theoretically, by increasing the etching rate (increasing the concentration of the H_2O_2 solution), a finer tube structure can be obtained.[6] Once the Ge sacrificial layer is totally etched away, the rolling-up process is over and the *h*-BN tube is formed.

Figure 2a,b respectively shows the optical microscopy image of the device before and after the rolling-up process, and the scanning electron microscopy (SEM) image of the tubular device is shown in Figure 2c. The rolled-up *h*-BN tube has a diameter of ≈10 µm. The device footprint area before the rolling-up process is about 0.003 mm^2, while the device footprint area of the rolled-up tube is about 0.0005 mm^2, which results in a reduction of ≈6 times (by increasing the length of the planar device, the reduction can be further improved). In order to explore the thickness of the *h*-BN, the height image of the transferred *h*-BN on the SiO_2 substrate was measured by atom force microscope (AFM). As plotted in Figure 2d, the extracted height difference between *h*-BN and the substrate shows the thickness of the *h*-BN film is about 6 nm. The inset of Figure 2d shows the AFM height image of *h*-BN on the SiO_2 substrate, and the bottom left part shows the *h*-BN film. Figure 2e is the Raman spectrum of the *h*-BN film on the SiO_2 substrate, and the excitation wavelength is 532 nm. The Raman spectrum shows a strong peak at 1366.38 cm^{-1}, which is basically consistent with the E_{2g} characteristic peak of *h*-BN in the previous studies.[30,34]

After the rolling-up process and characterization, the electrical properties of the tubular device were measured by semiconductor parameter analyzer. During the measurement, the

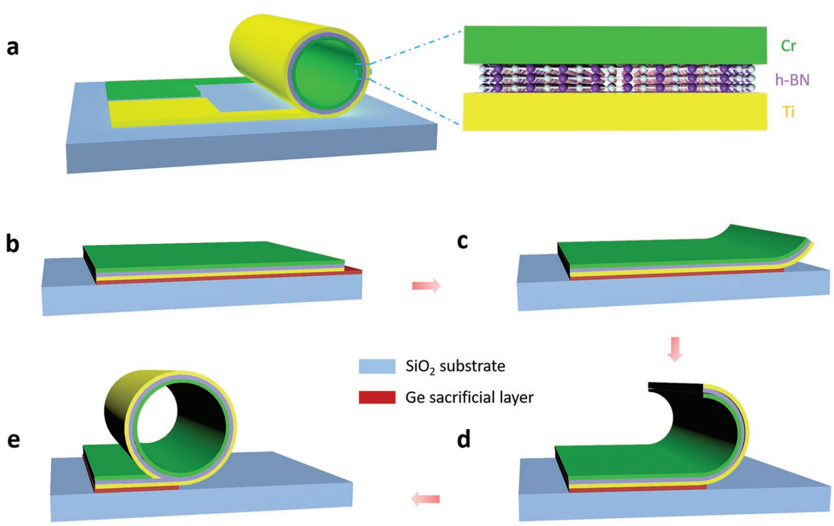

Figure 1. The 3D schematic representation and the rolling-up process of the *h*-BN tube (for intuitively display of the device structure, the second layer of *h*-BN is ignored in the 3D schematics, but it exists in the real device). a) 3D structure of the rolled-up *h*-BN tube on the SiO_2 substrate. Two contact pads are bonded on the substrate for electrical measurement after the device fabrication. The right part is the partial enlargement 3D schematic view of the tube, which represents a typical MIM structure. The bottom electrode is Ti and the top electrode is Cr, layered *h*-BN is caught between the bottom and top electrodes. b) The planar device after the RIE step, a trench is formed for the Ge sacrificial layer etching. c) When the Ge sacrificial layer is selectively etched by H_2O_2 solution, the device starts to release from the SiO_2 substrate forced by the strained layer. d,e) With the increase of the etching time, the strained layer stack gradually forms a 3D tubular structure.

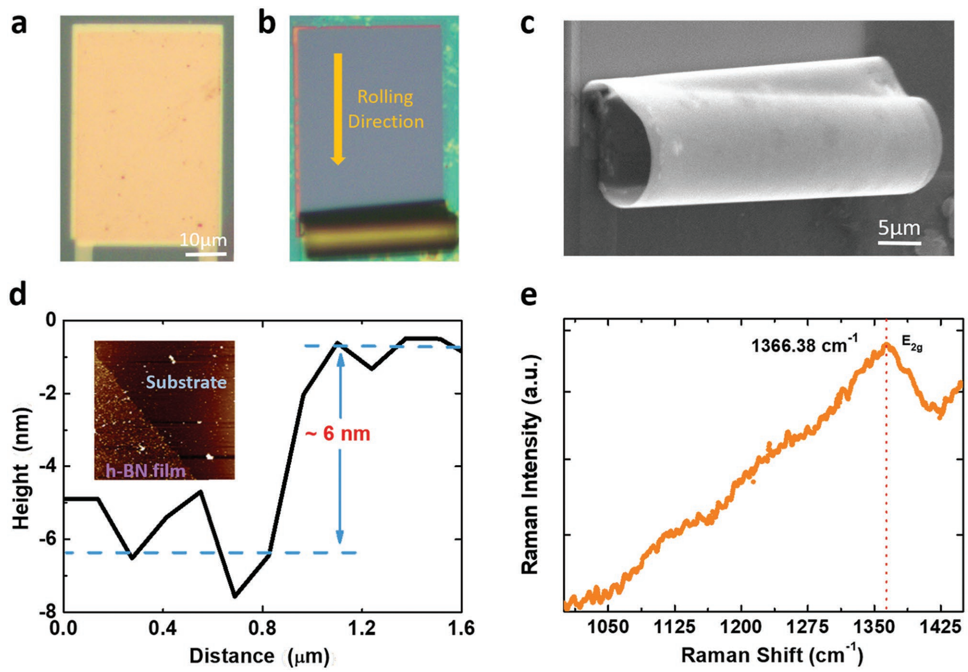

Figure 2. a) The optical microscopy image of the planar device, the scale bar is 10 μm. b) Optical microscopy image of the tubular device after the rolling-up process, the yellow arrow indicates the rolling direction in the process. c) The SEM image of the rolled-up *h*-BN tube, the scale bar is 5 μm. Diameter of the tube is about 10 μm. d) The extracted height data from the AFM height image of the *h*-BN film on the SiO_2 substrate, the height difference between the *h*-BN film and the substrate indicates that the thickness of the *h*-BN is about 6 nm. The inset is the AFM height image and the scale bar is 2 μm. e) Raman spectrum of the *h*-BN on the SiO_2 substrate, excited by 532 nm wavelength laser.

bias voltage was applied to the Ti electrode, and the Cr electrode was grounded. The typical *I–V* curve of the rolled-up *h*-BN tube is plotted in **Figure 3**a (the inset is the *I–V* curve plotted in linear scale) by DC voltage sweeping, which exhibits a bipolar resistive switching behavior. The device is in a high resistance state (HRS or OFF state) initially, and with the gradual increase of the applied voltage, the current shows a slow increase. Suddenly, the current increases to a high level state when the applied voltage approaches a threshold value (Set voltage), which indicates a resistive switching from the HRS to low resistance state (LRS or ON state). Conversely, when the applied reverse voltage is swept to a negative value, the current can turn back to HRS. Moreover, the first three *I–V* sweeping curves in the positive voltage range exhibit approximately the same Set voltage (see more details in Figure S4 in the Supporting Information), which indicates a forming-free property[35] of the rolled-up *h*-BN tube. Compared with the planar device, rolled-up *h*-BN tube exhibits higher Set voltage and lower programing current (reduced by more than two orders of magnitude), and it is briefly explained in the next part. The typical *I–V* curve of the planar device before the rolling-up process is shown in Figure S5 in the Supporting Information.

To further explore the memory performance of the rolled-up *h*-BN tube, a positive pulse (+8 V amplitude, duration of 80 ms) and a negative pulse (–8 V amplitude, duration of 80 ms) were applied to the Ti electrode to realize the write

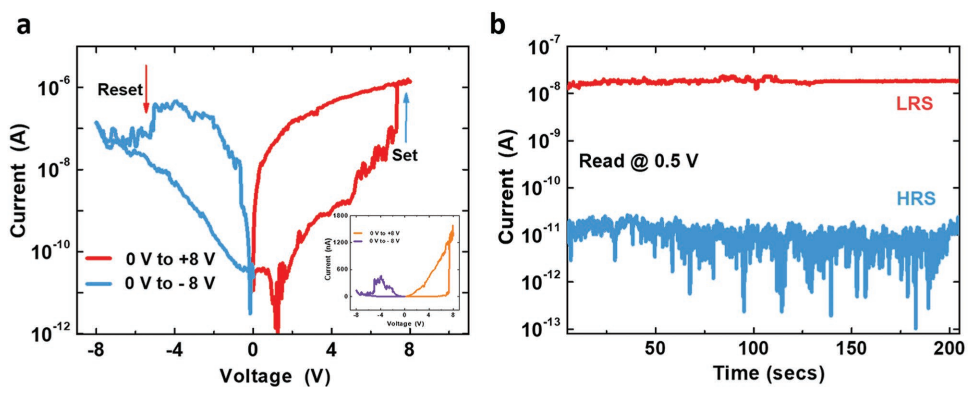

Figure 3. Resistive switching behavior of the rolled-up *h*-BN tube. a) The typical *I–V* curves of the tubular device, showing a bipolar-resistive switching behavior. The inset image is the *I–V* curves plotted in linear scale. b) Retention property of the LRS and HRS, the recording voltage is 0.5 V.

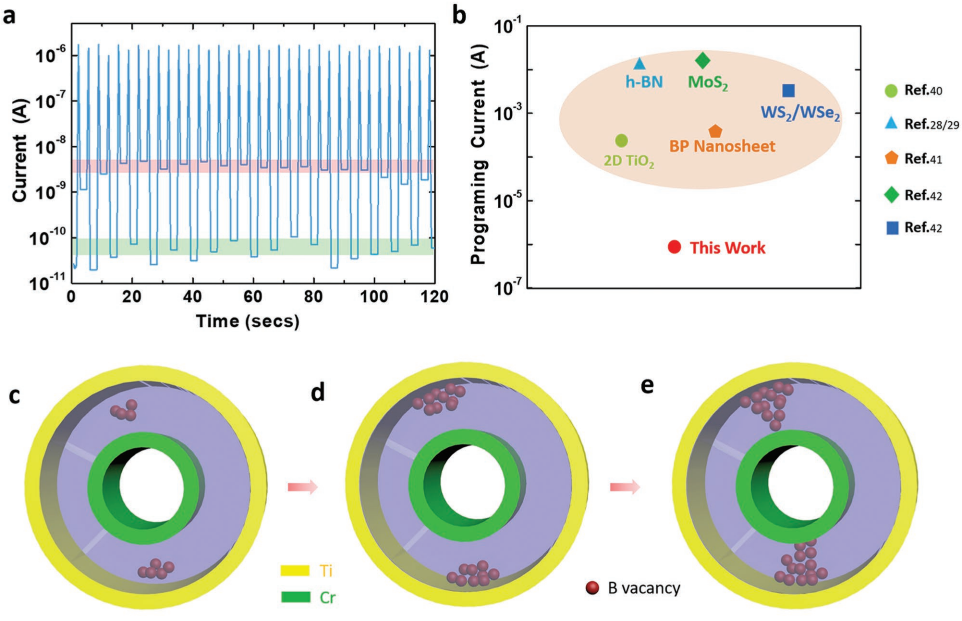

Figure 4. a) The dynamic response of the tubular memory device, the positive and negative pulses (± 8 V, 80 ms) are periodically applied to the device. After the pulse application, the current was monitored at 0.5 V voltage bias. b) Programing current summary of RRAM devices based on 2D materials. c–e) The formation process of the conductive filament in the rolled-up *h*-BN tube. The internal electrode is metal Cr, and the external is Ti. The red sphere represents the B vacancy.

and erase operation. Then, the current through the device was monitored with a recording voltage of 0.5 V at room temperature. As the curves plotted in Figure 3b, the ratio of the ON/OFF state current of the device can reach up to 10^3 with a nonvolatile property, which validates the potential of the rolled-up *h*-BN tube for data storage applications. **Figure 4**a shows the dynamic switching behavior of the device. The positive pulse (+8 V amplitude, duration of 80 ms) and negative pulse (–8 V amplitude, duration of 80 ms) were alternately applied to the Ti electrode, and the current through the *h*-BN was monitored at 0.5 V voltage bias between the positive pulse and negative pulse. The LRS and HRS are distinguished by the pink region and the green region. The current spikes were excited by the positive pulse and negative pulse. Based on the dynamic switching behavior, the endurance property of the device was extracted and plotted in Figure S6 in the Supporting Information.

Moreover, this tubular RRAM device exhibits satisfactorily low programing current (the current flow through the device during "Set" operation) compared with other planar 2D material-based RRAM devices, which is meaningful for RRAM applications. Cross-point memory technology is a promising building block for the next-generation nonvolatile memory applications. RRAM Cross-point memory building blocks are generally based on the one-selector-one-resistor (1S1R) configuration to mitigate the sneak-current problem.[36] For the 1S1R configuration, the voltage divider effect between the selector and the resistor should be minimized[[37] otherwise, the resistance mismatch between the selector and the resistor will lower the memory window (ON/OFF ratio) and reduce the memory performance.[37,38] There are two alternative ways to solve this problem: One is combining the RRAM device with a high-current density selector, and the other is integrating the selector with a low-current RRAM device.[39] However, the ON-state currents of the selectors are typically limited[37] and the high-current density results in high power consumption. Therefore, the development of low-current RRAM device is an appropriate method. Moreover, by integrating selector with low-current RRAM device, low power consumption can be maintained, which meets the demands of data storage applications.[39]

A comparison of this tubular RRAM device based on 2D *h*-BN and other planar 2D materials-based RRAM devices is shown in Figure 4b. The programing current of this tubular RRAM device is about 1 µA, which is lower than other RRAM devices based on 2D materials (2D TiO_2,[40] BP nano sheet,[41] *h*-BN,[28,29] MoS_2,[42] etc.). Thus, the rolled-up *h*-BN tube is promising for ideal 1S1R configuration and low power memory applications.

It is recognized by many researchers that the switching mechanism observed in RRAM devices based on TMOs are governed by O vacancies or metal ions movement, which is called the valence change mechanism (VCM).[43] Consider that the *h*-BN has similar properties to the TMOs, and the diffusion ability of the Ti and Cr electrodes are not strong, the resistive switching mechanism in the tubular RRAM device should be VCM.

Theoretically, as a type of 2D materials, *h*-BN should have an ideal layered and perfect lattice structure. Thus, the charge paths are difficult to form in *h*-BN. However, it has been previously reported that grain boundary defects exists in the CVD grown polycrystalline 2D *h*-BN films.[28,29] And the grain boundary defects are the B vacancies rich area,[29,44] this may be reason why the tubular RRAM device exhibits a forming-free behavior. When a positive voltage bias is applied to the Ti electrode, the B ions in the *h*-BN switching layer can migrate to the Ti/*h*-BN interface with the assist of the grain boundary defects and leave the B vacancies in the original position. Once the B vacancies arrive at the Cr electrode, the conductive filament is completely formed. As a result, the device switches from the HRS to LRS. The simulation process of the resistive switching mechanism is shown in Figure 4c to Figure 4e. In the initial state (no voltage applied to the device), few B vacancies are distributed in the *h*-BN film (Figure 4c). When a positive voltage is applied to the Ti electrode, the B ions near the Ti electrode move first and leave the B vacancies (Figure 4d). Finally, with the increase of the applied voltage, the B vacancies path arrives at the Cr electrode and a conductive filament is formed (Figure 4e). As shown in Figure S7 in the Supporting Information, after the formation of the conductive filament, the device shows approximately ohmic conduction behavior (slope of the ln (I) ~ ln (V) curve is about 1).

Different from the planar device, the electric field between the Ti and Cr electrodes in rolled-up tubular device is not uniformly distributed, and the electric field lines are not parallel to each other. As a result, the B vacancies' migration and the conductive filament's formation in the rolled-up *h*-BN switching layer are more difficult. That might be the reason why the rolled-up *h*-BN tube exhibits higher Set voltage and lower programing current.

In conclusion, tubular RRAM device with forming-free and bipolar resistive switching behavior was realized via rolled-up *h*-BN tube, which was obtained by self-rolled-up technology with a relatively smaller footprint area. The tubular RRAM device exhibited excellent memory performance, such as nonvolatile ability and satisfactorily low programing current. The rolled-up tubular RRAM has the potential for increasing the data storage density, reducing the power consumption in memory application, and may be applied in the fields of sensing-storage integration for 3D devices.

Experimental Section

Device Fabrication: The 15 nm thick Ge sacrificial layer was deposited on the Si/SiO_2 substrate by e-beam evaporation (TSV-100). After the Ge deposition, the patterns of the Au/Ti plate were defined by e-beam lithography. In the e-beam lithography process, a polymethyl methacrylate (PMMA) layer was spin coated on the substrate at 500 rpm for 10 s and 4000 rpm for 1 min. Then, the sample was baked for 3 min with a hot plate at 170 °C, and the exposure was realized by Hitachi SU1510. The Au/Ti plate consisted of 2 nm Au and 15 nm Ti were deposited by e-beam evaporation with a rate of 1 Å s^{-1}. The sample was sequentially immersed in acetone and baked for 10 min at 50 °C to remove the residual metal and photoresist.

The *h*-BN used in this study was grown on copper foils by CVD. A PMMA supporting layer was then spin coated onto the surface of *h*-BN. The PMMA/*h*-BN/Cu structure was sequentially immersed in the $FeCl_3$ solution (0.5 g mL^{-1}) to remove the Cu, and the PMMA/*h*-BN stack was repeatedly washed in deionized water. Then, the PMMA/*h*-BN stack was transferred onto the substrate with the Au/Ti plate. The precoated PMMA supporting layer was removed by acetone.

The Cr plate was deposited on the sample with a thickness of 15 nm and a deposition rate of 1.2 Å s^{-1} by e-beam evaporation. After that, the second layer *h*-BN was transferred onto the Cr plate. The patterns of the trench were defined by e-beam lithography, and the *h*-BN in the trench was etched away by RIE. To release the planar structure, the sample was immersed in a solution of H_2O_2:H_2O (1:50).

Atomic Force Microscopy: The AFM measurements were performed with the Bruker Veeco MultiMode 8 system. The height image of the sample was measured in the Tapping Mode. The height data were extracted by NanoScope Analysis software.

Scanning Electron Microscopy: The rolled-up tubular structure was imaged using Hitachi SU1510 with a 15 kV working voltage.

Electrical Measurement: The electrical performance of the devices was measured by Keithly 4200 SCAS semiconductor parameter analyzer.

Supporting Information

Supporting Information is available from the Wiley Online Library or from the author.

Acknowledgements

This work was supported by the National Natural Science Foundation of China (61622401, U1632115, and 61734003) and National Key Research and Development Program (2017YFB0405600, 2016YFA0203900). Y.F.M. thanks for the support from the Science and Technology Commission of Shanghai Municipality (17JC1401700) the Changjiang Young Scholars Program of China.

Conflict of Interest

The authors declare no conflict of interest.

Keywords

h-BN, resistive switching, self-rolled-up technology, tubular memory

Received: September 18, 2018
Revised: December 5, 2018
Published online: January 9, 2019

[1] R. Sharma, C. C. B. Bufon, D. Grimm, R. Sommer, A. Wollatz, J. Schadewald, D. J. Thurmer, P. F. Siles, M. Bauer, O. G. Schmidt, *Adv. Energy Mater.* **2014**, *4*, 1301631.
[2] Z. Tian, L. Zhang, Y. Fang, B. Xu, S. Tang, N. Hu, Z. An, Z. Chen, Y. Mei, *Adv. Mater.* **2017**, *29*, https://doi.org/10.1002/adma.201604572.
[3] W. Si, I. Mönch, C. Yan, J. Deng, S. Li, G. Lin, L. Han, Y. Mei, O. G. Schmidt, *Adv. Mater.* **2014**, *26*, 7973.
[4] J. Deng, X. Lu, L. Liu, L. Zhang, O. G. Schmidt, *Adv. Energy Mater.* **2016**, *6*, 1600797.
[5] C. Vervacke, C. C. B. Bufon, D. J. Thurmer, O. G. Schmidt, *RSC Adv.* **2014**, *4*, 9723.
[6] C. C. Bufon, J. D. González, D. J. Thurmer, D. Grimm, M. Bauer, O. G. Schmidt, *Nano Lett.* **2010**, *10*, 2506.
[7] D. Grimm, C. C. Bof Bufon, C. Deneke, P. Atkinson, D. J. Thurmer, F. Schäffel, S. Gorantla, A. Bachmatiuk, O. G. Schmidt, *Nano Lett.* **2013**, *13*, 213.
[8] H. X. Ji, X. L. Wu, L. Z. Fan, C. Krien, I. Fiering, Y. G. Guo, Y. Mei, O. G. Schmidt, *Adv. Mater.* **2010**, *22*, 4591.
[9] C. Yan, W. Xi, W. Si, J. Deng, O. G. Schmidt, *Adv. Mater.* **2013**, *25*, 539.
[10] W. Huang, X. Yu, P. Froeter, R. Xu, P. Ferreira, X. Li, *Nano Lett.* **2012**, *12*, 6283.
[11] S. Miao, D. Chen, A. Madani, M. R. Jorgensen, V. A. Bolaños Quiñones, L. Ma, S. G. Hickey, A. Eychmüller, O. G. Schmidt, *Adv. Opt. Mater.* **2015**, *3*, 187.

[12] P. Ball, *Nature* **1999**, *399*, 729.
[13] D. Cooper, C. Baeumer, N. Bernier, A. Marchewka, C. L. Torre, R. E. Dunin-Borkowski, S. Menzel, R. Waser, R. Dittmann, *Adv. Mater.* **2017**, *29*.
[14] W. A. Hubbard, A. Kerelsky, G. Jasmin, E. R. White, J. Lodico, M. Mecklenburg, B. C. Regan, *Nano Lett.* **2015**, *15*, 5665.
[15] C. Gopalan, Y. Ma, T. Gallo, J. Wang, E. Runnion, J. Saenz, F. Koushan, P. Blanchard, S. Hollmer, *Solid-State Electron.* **2010**, *58*, 54.
[16] D. H. Kwon, K. M. Kim, J. H. Jang, J. M. Jeon, M. H. Lee, G. H. Kim, X. S. Li, G. S. Park, B. Lee, S. Han, *Nat. Nanotechnol.* **2010**, *5*, 148.
[17] Y. Wu, B. Lee, H. S. P. Wong, *IEEE Electron Device Lett.* **2010**, *31*, 1449.
[18] L. Chen, H. Y. Gou, Q. Q. Sun, P. Zhou, H. L. Lu, P. F. Wang, S. J. Ding, D. W. Zhang, *IEEE Electron Device Lett.* **2011**, *32*, 794.
[19] H. Y. Lee, P. S. Chen, T. Y. Wu, Y. S. Chen, C. C. Wang, P. J. Tzeng, C. H. Lin, F. Chen, C. H. Lien, M. J. Tsai, presented at *2008 IEEE Int. Electron Devices Meeting (IEDM)*, San Francisco, CA, USA, 15–17 December **2008**.
[20] K. G. Young-Fisher, G. Bersuker, B. Butcher, A. Padovani, L. Larcher, D. Veksler, D. C. Gilmer, *IEEE Electron Device Lett.* **2013**, *34*, 750.
[21] C. Lee, X. Wei, J. W. Kysar, J. Hone, *Science* **2008**, *321*, 385.
[22] X. Cui, G. H. Lee, Y. D. Kim, G. Arefe, P. Y. Huang, C. H. Lee, D. A. Chenet, X. Zhang, L. Wang, F. Ye, *Nat. Nanotechnol.* **2015**, *10*, 534.
[23] K. S. Novoselov, A. K. Geim, S. V. Morozov, D. Jiang, Y. Zhang, S. V. Dubonos, I. V. Grigorieva, A. A. Firsov, *Science* **2004**, *306*, 666.
[24] J. Wang, Q. Yao, C. W. Huang, X. Zou, L. Liao, S. Chen, Z. Fan, K. Zhang, W. Wu, X. Xiao, *Adv. Mater.* **2016**, *28*, 8302.
[25] Y. Ji, C. Pan, M. Zhang, S. Long, X. Lian, F. Miao, F. Hui, Y. Shi, L. Larcher, E. Wu, *Appl. Phys. Lett.* **2016**, *108*, 73103.
[26] K. Watanabe, T. Taniguchi, H. Kanda, *Nat. Mater.* **2004**, *3*, 404.
[27] K. K. Kim, A. Hsu, X. Jia, S. M. Kim, Y. Shi, M. Dresselhaus, T. Palacios, J. Kong, *ACS Nano* **2012**, *6*, 8583.
[28] C. Pan, Y. Ji, N. Xiao, F. Hui, K. Tang, Y. Guo, X. Xie, F. M. Puglisi, L. Larcher, E. Miranda, *Adv. Funct. Mater.* **2017**, *27*, 1604811.
[29] F. M. Puglisi, L. Larcher, C. Pan, N. Xiao, Y. Shi, F. Hui, M. Lanza, presented at *2016 IEEE Int. Electron Devices Meeting (IEDM)*, San Francisco, CA, USA, 3–7 December **2016**.
[30] L. Song, L. Ci, H. Lu, P. B. Sorokin, C. Jin, J. Ni, A. G. Kvashnin, D. G. Kvashnin, J. Lou, B. I. Yakobson, *Nano Lett.* **2010**, *10*, 3209.
[31] M. Chhowalla, H. S. Shin, G. Eda, L. J. Li, K. P. Loh, H. Zhang, *Nat. Chem.* **2013**, *5*, 263.
[32] R. Songmuang, C. Deneke, O. G. Schmidt, *Appl. Phys. Lett.* **2006**, *89*, 493.
[33] O. G. Schmidt, N. Y. Jin-Phillipp, *Appl. Phys. Lett.* **2001**, *78*, 3310.
[34] Y. Shi, C. Hamsen, X. Jia, K. K. Kim, A. Reina, M. Hofmann, A. L. Hsu, K. Zhang, H. Li, Z. Y. Juang, *Nano Lett.* **2010**, *10*, 4134.
[35] Y. S. Chen, H. Y. Lee, P. S. Chen, T. Y. Wu, C. C. Wang, P. J. Tzeng, F. Chen, M. J. Tsai, C. Lien, *IEEE Electron Device Lett.* **2010**, *31*, 1473.
[36] R. Aluguri, T. Y. Tseng, *IEEE J. Electron Devices Soc.* **2016**, *4*, 294.
[37] J. Zhou, K. H. Kim, W. Lu, *IEEE Trans. Electron Devices* **2014**, *61*, 1369.
[38] L. Zhang, S. Cosemans, D. J. Wouters, G. Groeseneken, M. Jurczak, B. Govoreanu, *IEEE Electron Device Lett.* **2015**, *36*, 570.
[39] J. Zhou, F. Cai, Q. Wang, B. Chen, S. Gaba, W. D. Lu, *IEEE Electron Device Lett.* **2016**, *37*, 404.
[40] Y. Dai, W. Bao, L. Hu, C. Liu, X. Yan, L. Chen, Q. Sun, S. Ding, P. Zhou, D. W. Zhang, *2D Mater.* **2017**, *4*, 025012.
[41] C. Hao, F. Wen, J. Xiang, S. Yuan, B. Yang, L. Li, W. Wang, Z. Zeng, L. Wang, Z. Liu, *Adv. Funct. Mater.* **2016**, *26*, 2016.
[42] R. Ge, X. Wu, M. Kim, J. Shi, S. Sonde, L. Tao, Y. Zhang, J. C. Lee, D. Akinwande, *Nano Lett.* **2017**, *18*, 434.
[43] I. Valov, E. Linn, S. Tappertzhofen, S. Schmelzer, J. V. D. Hurk, F. Lentz, R. Waser, *Nat. Commun.* **2013**, *4*, 1771.
[44] A. Zobelli, C. P. Ewels, A. Gloter, G. Seifert, *Phys. Rev. B* **2009**, *75*, 094104/1.